Composite pulses for ultrabroad-band and ultranarrow-band excitation

B. T. Torosov,[1,*] E. S. Kyoseva,[1] and N. V. Vitanov[2]

[1]*Engineering Product Development, Singapore University of Technology and Design, 8 Somapah Road, 487372 Singapore*

[2]*Department of Physics, St. Kliment Ohridski University of Sofia, 5 James Bourchier Boulevard, 1164 Sofia, Bulgaria*

(Received 30 January 2015; revised manuscript received 23 July 2015; published 8 September 2015)

We introduce ultrabroad-band composite pulses (CPs), which maximize (at the expense of a finite error tolerance ϵ) the pulse area range wherein the population inversion remains above $1-\epsilon$. We present such CPs for error thresholds $\epsilon = 0.01$, 0.001, and 0.0001 in two versions: CPs with different pulse areas of the constituent pulses, used as control parameters, and with equal pulse areas. The former CPs naturally outperform the CPs of identical pulses, which in turn outperform conventional broad-band CPs obtained by annulling the population inversion derivatives at a single point. Moreover, we derive double-compensation CPs, which correct errors in both the pulse area and the detuning. They outperform the corresponding conventional CPs as well. By using the same error-tolerance approach, we construct ultranarrow-band CPs, which squeeze the population inversion in as narrow a range as possible while keeping the excitation outside this range below the error threshold ϵ.

DOI: 10.1103/PhysRevA.92.033406 PACS number(s): 32.80.Qk, 42.50.Dv, 42.65.Re, 82.56.Jn

I. INTRODUCTION

The technique of composite pulses (CPs) is a powerful tool for quantum control and modular design of interactions. It has been widely used in nuclear magnetic resonance [1–4] and more recently in quantum optics [5–10] and quantum information [11–13]. The main advantage of CPs over other control techniques is that they combine high control accuracy with robustness to variations in one or more experimental parameters. A CP is a sequence of pulses with suitably chosen relative phases. These phases are used as control parameters to correct the errors that emerge in the interaction between a single pulse and a qubit or to shape up the excitation profile in a desired manner. Usually this is done by cancellation of propagator elements and their derivatives versus a particular parameter at a specific value of this parameter. In such a way one can produce a huge variety of broad-band (BB) [7,8,14–16], narrow-band (NB) [14,16–19], and passband [16,20,21] CPs. Moreover, in so doing one obtains CPs that produce extremely high accuracy (e.g., error below 10^{-10}) around the chosen parameter value. However, such extreme accuracy is barely needed, even in quantum information, wherein the usual error target is 10^{-4}. In more conventional applications, even accuracy of 99% usually suffices. The extreme accuracy of such CPs is therefore unnecessary and moreover it is costly, for it restricts the bandwidth of the profile. We note here that most of the results in the CP literature focus on two-state systems and only limited research has been focused on multilevel systems [6,22].

Here we present a different approach for construction of CPs, which trades accuracy for bandwidth. The method uses numerical optimization of the transition probability, with the objective to create as broad an excitation profile as possible for ultrabroad-band (UBB) CPs [or as narrow as possible for ultranarrow-band (UNB) CPs], at the expense of a higher error tolerance. In addition to the increased (for BB) or reduced (for NB) bandwidth, this method allows us to reduce the total pulse area and in such a way to create robust CPs of fairly small pulse area. As benchmarks for comparison we use the BB and NB CPs derived recently [7,19] because their phases are given by analytic formulas for any number of pulses and particularly because they have been shown to perform equally well or outperform the previous CPs with the same number of pulses. We extend this approach to double compensation of the pulse area and detuning errors wherein we use as a benchmark the universal CPs [10], which allow for compensation of errors in multiple interaction parameters.

The paper is organized as follows. In Sec. II we start with a brief overview of the theory of CPs. Then, in Sec. III we explain how we can boost the bandwidth of the standard CPs by introducing a finite error. We calculate the composite phases for several particular examples and compare the results with those for the standard CPs. Ultranarrow-band CPs are presented in Sec. IV. Finally, in Sec. V we summarize the results.

II. STANDARD COMPOSITE PULSES

To explain the idea of CPs, let us consider a two-state quantum system (a qubit), in a general state $|\Psi\rangle = c_1|\psi_1\rangle + c_2|\psi_2\rangle$, interacting with an external coherent field. The evolution of the qubit is described by the Schrödinger equation

$$i\hbar\partial_t \mathbf{c}(t) = \mathbf{H}(t)\mathbf{c}(t), \tag{1}$$

where $\mathbf{c}(t) = [c_1(t), c_2(t)]^T$ is a column vector with the probability amplitudes of the two states $|\psi_1\rangle$ and $|\psi_2\rangle$. The Hamiltonian after the rotating-wave approximation [23] is

$$\mathbf{H}(t) = (\hbar/2)\Omega(t)e^{-iD(t)}|\psi_1\rangle\langle\psi_2| + \text{H.c.}, \tag{2}$$

with $D = \int_0^t \Delta(t')dt'$, where $\Delta = \omega_0 - \omega$ is the detuning between the field frequency ω and the Bohr transition frequency ω_0. The Rabi frequency $\Omega(t)$ is a measure of the field-system interaction: For laser-driven electric dipole atomic transitions $\Omega(t) = -\mathbf{d}\cdot\mathbf{E}(t)/\hbar$, where $\mathbf{E}(t)$ is the laser electric-field envelope and $\mathbf{d}$ is the transition dipole moment of the atom. It is convenient to describe the evolution of the quantum system by means of the propagator $\mathbf{U}(t,t_i)$, which

*Permanent address: Institute of Solid State Physics, Bulgarian Academy of Sciences, 72 Tsarigradsko Chaussée, 1784 Sofia, Bulgaria.

connects the probability amplitudes at any given time t to their initial values at time t_i: $\mathbf{c}(t) = \mathbf{U}(t,t_i)\mathbf{c}(t_i)$. For the sake of simplicity, hereafter we drop the temporal arguments in $\mathbf{U}$. Because the 2×2 propagator is unitary it can be parametrized by two complex Cayley-Klein parameters a and b as

$$\mathbf{U} = \begin{bmatrix} a & b \\ -b^* & a^* \end{bmatrix}. \tag{3}$$

A constant phase shift ϕ in the driving field $\Omega(t) \to \Omega(t)e^{i\phi}$ is mapped onto the propagator as

$$\mathbf{U}(\phi) = \begin{bmatrix} a & be^{i\phi} \\ -b^*e^{-i\phi} & a^* \end{bmatrix}. \tag{4}$$

We assume resonant excitation ($\Delta = 0$) hereafter; for a resonant pulse of pulse area A we have $a = \cos(A/2)$ and $b = -i\sin(A/2)$. A sequence of N identical pulses, each with a different phase ϕ_k, produces a CP whose effect upon the quantum system is described by the propagator

$$\mathbf{U}^{(N)} = \mathbf{U}(\phi_N)\cdots\mathbf{U}(\phi_2)\mathbf{U}(\phi_1). \tag{5}$$

When the system is initially in state $|1\rangle$, the transition probability is $\mathcal{P} = |U_{21}^{(N)}|^2$ and the probability for no transition is $\mathcal{Q} = 1 - \mathcal{P} = |U_{11}^{(N)}|^2$. Complete population inversion means $\mathcal{P} = 1$ and hence $\mathcal{Q} = 0$.

If the phases ϕ_k are chosen appropriately one can modify the excitation profile essentially in any desired manner. In particular, one can nullify the first few terms in the Taylor expansion of the propagator against a certain parameter at a specific value. Thereby the total propagator can be made much more robust to variations in this parameter than the single-pulse propagator $\mathbf{U}$. Composite pulses can be made robust to variations in essentially any desired experimental parameter as well as in several parameters simultaneously.

The CPs derived by cancellation of Taylor coefficients (i.e., probability derivatives) at the selected parameter value produce excitation profiles of extremely high accuracy, which may not be necessary in some applications. In the following sections we show that if a higher error ($\epsilon < 10^{-n}$, with $n = 2,3,4$) is tolerated, one can obtain CPs with even higher robustness of the profiles, i.e., with broader intervals of parameter values wherein the error remains below the selected value. We refer to these CPs as UBB and UNB pulses.

III. ULTRABROAD-BAND COMPOSITE PULSES

A. Nonidentical pulses

1. Numerical method

We begin by outlining the method that we use to derive the UBB CPs for complete population inversion. The condition for identical pulses in the composite sequence is convenient in some implementations, but it is not mandatory in general. Here we present composite sequences of pulses of different areas $A_1, A_2, \ldots, A_N$, which are more efficient than sequences of identical pulses. We denote such sequences by (acting from left to right)

$$(A_1)_{\phi_1}(A_2)_{\phi_2}\cdots(A_N)_{\phi_N} \tag{6}$$

and the overall propagator reads

$$\mathbf{U}^{(N)} = \mathbf{U}(A_N,\phi_N)\cdots\mathbf{U}(A_2,\phi_2)\mathbf{U}(A_1,\phi_1), \tag{7}$$

where on exact resonance the single-pulse propagator is

$$\mathbf{U}(A,\phi) = \begin{bmatrix} \cos(A/2) & -ie^{i\phi}\sin(A/2) \\ -ie^{-i\phi}\sin(A/2) & \cos(A/2) \end{bmatrix}. \tag{8}$$

The transition probability generated by the CP reads $\mathcal{P} = |U_{12}^{(N)}|^2$ and the no-transition probability is $\mathcal{Q} = 1 - \mathcal{P} = |U_{11}^{(N)}|^2$. We assume that all areas deviate simultaneously,

$$A_k = a_k\alpha, \tag{9}$$

where α is the deviation factor and a_k are fixed numbers that determine the relative pulse areas and vary for each CP; these numbers are derived numerically. The objective is, by varying the numbers a_k and the phases ϕ_k ($k = 1,2,\ldots,N$), to maximize the range of pulse areas (i.e., the range of values of the parameter α) wherein the transition probability remains above the value $1 - \epsilon$, i.e., the no-transition probability stays below ϵ: $\mathcal{Q} < \epsilon$, where ϵ is the selected error tolerance level.

We proceed as follows. For a given number of pulses N, we calculate (using *Mathematica*) the no-transition probability $\mathcal{Q} = |U_{11}^{(N)}|^2$ from Eq. (7). Thereby we obtain a cumbersome expression that depends on the numbers a_k and the phases ϕ_k. Next we calculate the width of the interval $(\alpha_{\min},\alpha_{\max})$, wherein the no-transition probability $\mathcal{Q}(\alpha)$ remains below the selected error threshold ϵ at all points of this interval,

$$\max\{\mathcal{Q}(\alpha)\} < \epsilon, \quad [\alpha \in (\alpha_{\min},\alpha_{\max})]. \tag{10}$$

Of particular significance are the dynamic range ratio

$$r = \frac{\alpha_{\max}}{\alpha_{\min}}, \tag{11}$$

which determines the bandwidth of the profile, and the minimum total pulse area

$$A_{\min} = \sum_{k=1}^{N} A_{k,\min} = \alpha_{\min}\sum_{k=1}^{N} a_k, \tag{12}$$

which corresponds to the lower bound of the high-fidelity interval $(\alpha_{\min},\alpha_{\max})$. Here $A_{\min}$ determines the maximum speed of the CP inversion. For each selected number of pulses N and each error threshold ϵ, we maximize numerically (by varying the parameters a_k and the phases ϕ_k) the dynamic range r, for which the no-transition probability $\mathcal{Q}$ at all points in the interval $(\alpha_{\min},\alpha_{\max})$ remains below ϵ, while pushing the total area to as small values as possible.

2. Ultrabroad-band composite pulse sequences

The UBB CPs derived by this method are listed in Table I in the Appendix. We denote them by UBN (ultrabroad-band composite sequence of N pulses) and group them in three categories in regard to the maximum admissible error ϵ. The figure of merit is the dynamic range ratio r, which naturally increases with the number of constituent pulses N in the CP sequence. The UB3 CPs use identical pulses (of equal area), whereas the higher CPs involve pulses of unequal areas; however, the area ratios are rational numbers. We note also that for odd N the CPs are symmetric, while for even N

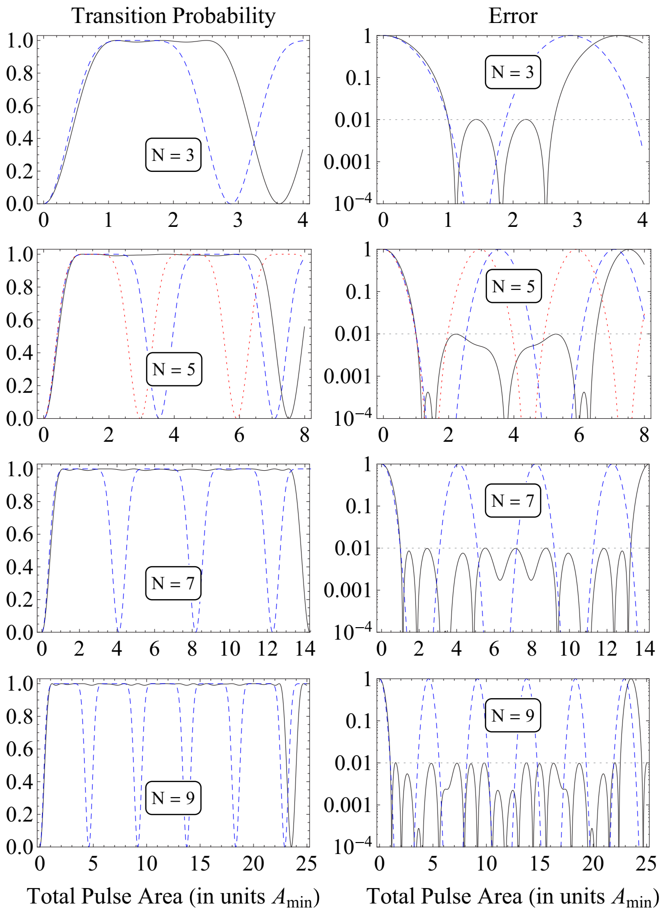

FIG. 1. (Color online) Transition probability $\mathcal{P}$ (left column) and infidelity (error) $\mathcal{Q} = 1 - \mathcal{P}$ (right column) vs the total pulse area for the UBB CPs UBN, with $N = 3,5,7,9$ (solid lines). The parameters of these CPs are given in Table I (tolerated error $\epsilon = 0.01$). The dashed lines show the profiles of the ordinary BB CPs with the phases of Eq. (13) [7]. The dotted red line in the $N = 5$ frames represents the transition profile for the BB1 composite pulse of Wimperis [16].

they are asymmetric. These features have emerged from the numerical maximization of r and they are not set beforehand. The minimum total pulse area is very modest: It does not exceed 4π, 4.5π, and 5π for $\epsilon = 0.01$, 0.001, and 0.0001, respectively. It is especially remarkable that with UBB CPs of six or more pulses, a transition probability $\mathcal{P} > 0.99$ is achieved for couplings in huge ranges differing by a factor of 10 and more. Especially impressive is the staggering value of r of 22.5 for UB9: In terms of the interaction of a two-level atom with a quantized light field, this covers a huge range of coupling constants (proportional to $\sqrt{n+1}$) for photon numbers from $n = 0$ to nearly $n = 500$. A range r of over 10 is achieved by the UB9 pulse even for transition probability $\mathcal{P} > 0.999$.

As a benchmark for comparison we use the BN broadband pulses we have derived earlier [7]. They are sequences of N identical pulses (with N odd), with phases

$$\phi_k = \frac{k(k-1)\pi}{N} \quad (k = 1,2,\ldots,N). \tag{13}$$

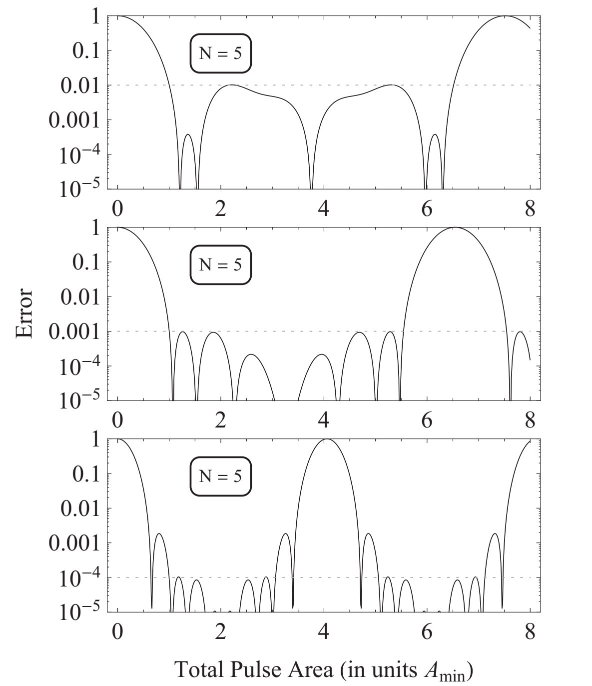

FIG. 2. Population inversion error $\mathcal{Q} = 1 - \mathcal{P}$ vs the total pulse area for the UBB CPs UB5 for different values of the tolerated error ϵ. The parameters of these UBB CPs are given in Table I.

The no-transition probability for these CPs is $\mathcal{Q} = \cos^{2N}(A/2)$ [20], where A is the pulse area of each pulse. From here we can easily calculate the dynamic range of these CPs for each ϵ and each N, which is

$$r = \frac{\pi}{\arccos(\epsilon^{1/2N})} - 1. \tag{14}$$

This formula is valid for a single pulse ($N = 1$) as well; it gives $r = 1.14$, 1.04, and 1.013 for $\epsilon = 0.01$, 0.001, and 0.0001, respectively. One can verify that the dynamic ranges of the UBN CPs listed in Table I exceed considerably those of the regular BN CPs. For example, for $\epsilon = 0.01$ we find $r = 1.89$, 2.54, 3.09, 3.58, and 4.03 for B3, B5, B7, B9, and B11 CPs, respectively; these values are far below those for the respective UBN CPs.

Several excitation profiles are depicted in Fig. 1. For the sake of easy comparison, the total pulse area of the sequence $\sum_{k=1}^{N} A_k$ is measured in units $A_{\min}$, so the high-fidelity window extends from 1 to r. As one can see, the UBB CPs are much broader than the corresponding BB CPs. In order to get a feeling for the extent of improvement of the high-fidelity range by our UBB CPs, we have also added in the $N = 5$ frames the well-known BB1 composite pulse of Wimperis [16].

Figure 2 shows the error of three inversion profiles for UB5 CPs with different error threshold ϵ. Naturally, the larger the tolerated error ϵ, the broader the corresponding inversion profile.

B. Identical pulses

In some applications it may be more convenient, or only possible, to use identical pulses, with the same pulse area. It is still possible to construct UBB CPs of greater bandwidth than the standard BB CPs, although of lesser bandwidth compared to the UBB CPs with nonidentical pulses. Looking back at Eq. (9), we see that the condition for identical pulses amounts to setting all numbers $a_k = 1$ ($k = 1,2,\ldots,N$). Then the area parameter α is equal to the area of each constituent pulse in the CP.

For a sequence of N identical resonant pulses of pulse area α each but with different phases,

$$\alpha_{\phi_1}\alpha_{\phi_2}\cdots\alpha_{\phi_N}, \tag{15}$$

the total propagator is given by Eq. (5). We use the same numerical method for the derivation of these UBB CPs as the one for the UBB CPs with unequal areas above. Numerical evidence suggests that the composite phases must satisfy the anagram condition $\phi_k = \phi_{N-k+1}$ ($k = 1,2,\ldots,N$). Moreover, we have found that the CPs with an even number of pulses do not outperform than the CPs with a smaller odd number of pulses; hence we only consider here odd N.

We present the derived UBB CPs in Table II in the Appendix. The dynamic range ratio r is a factor of 1.5–2 lower than for the UBB CPs with nonidentical pulses in Table I. Still, the values of r are substantially higher than the ones for the conventional BB CPs [cf. Eq. (14)]. Several excitation profiles are depicted in Fig. 3. As one can see, the UBB CPs are much broader than the conventional BB CPs but still, they are outperformed by the UBB CPs with nonidentical pulses shown in Fig. 1.

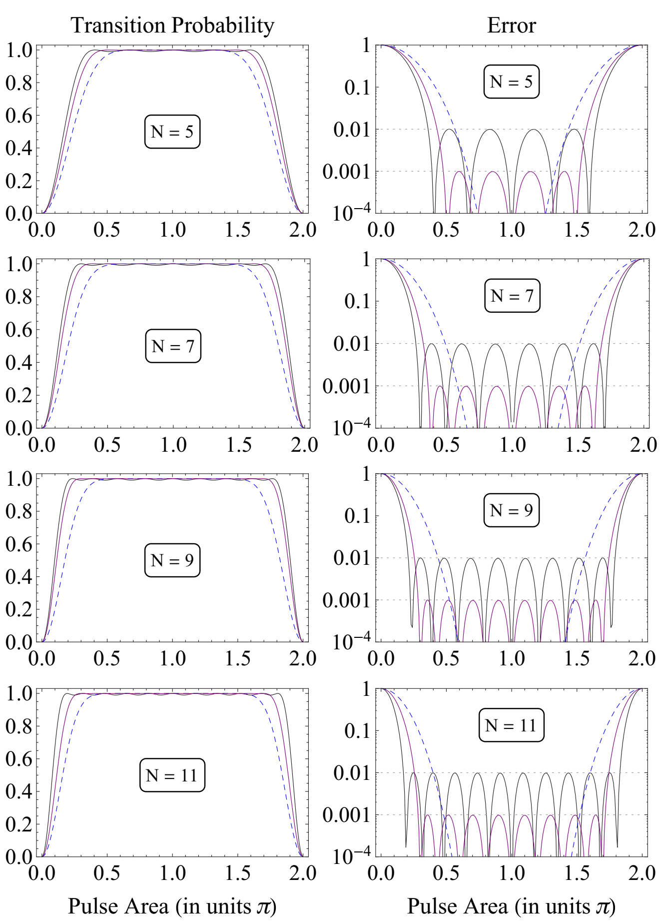

FIG. 3. (Color online) Transition probability $\mathcal{P}$ (left column) and infidelity (error) $\mathcal{Q} = 1 - \mathcal{P}$ (right column) vs the single-pulse area α for the UBB CPs composed of identical pulses, for $N = 5,7,9,11$ (solid lines). The composite phases are given in Table II and the tolerated error is set to $\epsilon = 0.01$ and 0.001. The dashed blue lines compare the profiles of the corresponding standard BB CPs, with phases, taken from [7].

C. Ultrabroad-band composite sequences for double compensation

The proposed technique can be extended to derive ultrabroad-band composite pulses, which produce excitation profiles robust against more than a single parameter. Here we present composite sequences that perform double compensation of errors in the pulse area and the detuning. This is done by numerical maximization of the area in the 2D space (Ω,Δ), in which the transition probability remains above $1-\epsilon$.

Table III shows such composite pulses for sequences of three, five, seven, and nine pulses. The efficiency of these CPs is shown in Fig. 4. For any value of the admissible error ϵ, the high-fidelity area for the UBB CPs is vastly expanded compared to the universal CPs [10] for $N = 3$, 7, and 9 pulses and moderately increased for $N = 5$ pulses.

Our numerical maximization method allows a far greater flexibility compared to previous methods because the high-fidelity area can be shaped in essentially any desired manner. We illustrate this tunability in Fig. 5, where three different five-pulse UBB CPs are shown to produce three different profiles: (i) a balanced profile with equal compensation of errors in Δ and Ω (the same as in Fig. 4), (ii) an elongated detuning-biased profile, which has an enhanced fidelity range vs Δ, and (iii) an elongated area-biased profile, which has an enhanced fidelity range vs Ω.

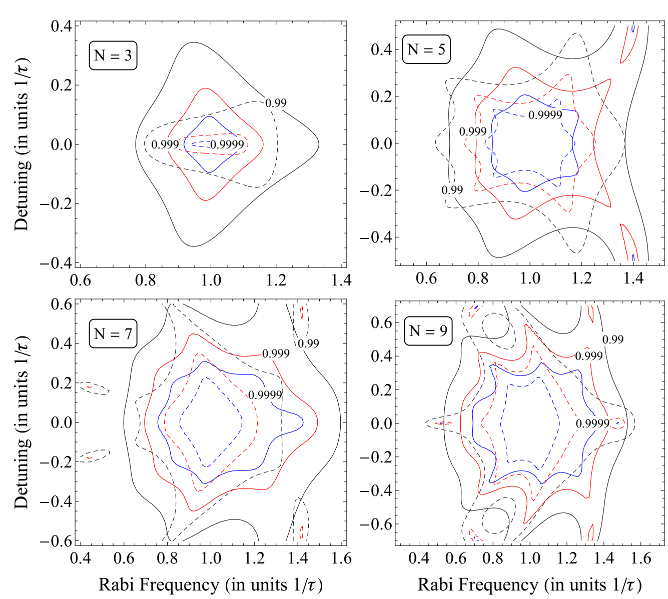

FIG. 4. (Color online) Transition probability $\mathcal{P}$ vs the Rabi frequency and the detuning for the UBB CPs for double-compensation with three, five, seven, and nine pulses given in Table III. The solid lines correspond to different values of the tolerated error $\epsilon = 0.0001$, 0.001, and 0.01 (from the inside outward). The dashed lines are the corresponding lines for the universal CPs of Ref. [10].

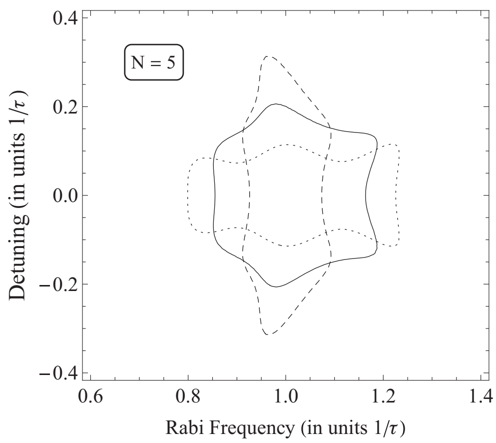

FIG. 5. Transition probability $\mathcal{P}$ vs the Rabi frequency and the detuning for the UBB CPs for a composite sequence of five pulses with different optimization shapes. The tolerated error is set to $\epsilon = 0.0001$ and the corresponding CPs are given in Table III (UB5, UB5d, and UB5a) are depicted by solid, dashed and dotted curves, respectively.

IV. ULTRANARROW-BAND COMPOSITE PULSES

The UNB CPs are derived in a similar way to the UBB ones. This time we force the excitation probability $\mathcal{P}$ to remain below the value ϵ in as broad intervals on the two sides of the central peak as possible. Numerical simulations return sequences of identical pulses with the same pulse area but different (nonanagram) phases. As in the previous section, we derive the phases for $N = 3$, 5, 7, 9, and 11. We list these results in Table IV, where we also show the ratio r between the right and left borders, outside of which the error is below the chosen threshold. A smaller r means a better NB sequence.

As a benchmark for comparison we use the NN narrowband pulses we have derived earlier [19]. They are sequences of N identical pulses (with N odd), with phases

$$\phi_{2k} = -\phi_{2k+1} = \frac{2k\pi}{N} \quad [k = 0,1,\ldots,(N-1)/2]. \tag{16}$$

The transition probability is $\mathcal{P} = \sin^{2N}(\alpha/2)$ [19], where α is the pulse area of each pulse. From here we calculate the dynamic range of these CPs, which is

$$r = \frac{\pi}{\arcsin(\epsilon^{1/2N})} - 1. \tag{17}$$

One can verify that the dynamic ranges of the UNN CPs listed in Table IV outperform considerably those of the regular NB CPs. For example, for $\epsilon = 0.01$ we find $r = 5.51$, 3.60, 2.91, 2.55, and 2.32 for N3, N5, N7, N9, and N11 CPs, respectively; these values are far above those for the respective UNN CPs.

The excitation profiles of these UNB CPs are plotted in Fig. 6. Again, the superiority of the UNB CPs over the NB CPs is obvious.

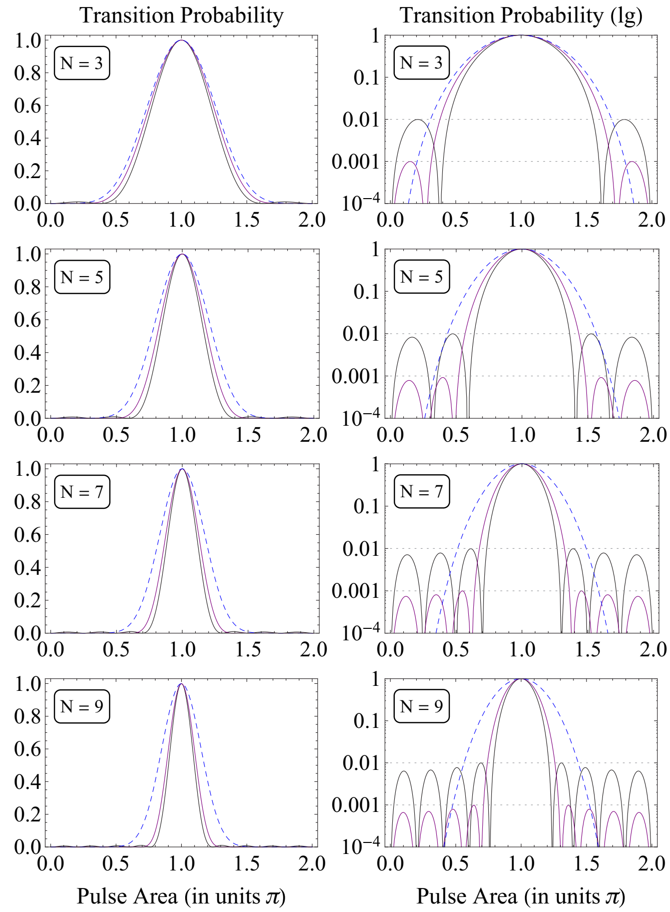

FIG. 6. (Color online) Transition probability $\mathcal{P}$ on an absolute scale (left column) and on a logarithmic scale (right column) as a function of the single-pulse area for the UNB CPs, for $N = 3,5,7,9$ (solid lines). The error tolerance is $\epsilon = 0.01$ and 0.001 and the composite phases are given in Table IV. The dashed lines show the profiles of the corresponding standard NB CPs with the phases of Eq. (16) [19].

V. CONCLUSION

We have presented an approach to construct UBB CPs, which produce much broader excitation profiles than the traditional CPs at the expense of a finite error ϵ in the high-probability range, that is the range of pulse areas in which the transition probability remains above $1 - \epsilon$. As a quality measure for these CPs we have adopted the ratio r [Eq. (11)] between the upper and lower bounds of this range. This ratio tells us how broad the range of couplings is for which efficient excitation can occur simultaneously. We have constructed such CPs for error thresholds $\epsilon = 0.01$, 0.001, and 0.0001 in two variations: with constituent pulses of different and equal pulse areas, the former being superior in terms of bandwidth. Both types considerably outperform the conventional single-point broad-band CPs. For example, for error level $\epsilon = 0.01$ the dynamic range r varies from 3.6 for the conventional B9 pulse to 8.6 for the ultrabroad-band UB9e composed of identical pulses and 22.5 for the ultrabroad band UB9 composed of nonidentical pulses. In another example, in order to produce excitation above 99% for couplings differing by up to a factor of $r = 4$, one needs the 11-pulse single-point B11 sequence, while only the four-pulse UBB pulse UB4 suffices for the same objective.

By using the same method we have constructed also UNB CPs, which outperform the conventional single-point NB CPs too. It is important to note that the presented UBB and UNB CPs can be used as building modules to design higher CPs, by using the nesting technique, where a larger CP is constructed by nesting shorter CPs of identical pulses [14,16–18,20,21]. For instance, an N-pulse CP with phases ϕ_j ($j = 1,2,\ldots,N$) nested in an M-pulse CP with phases χ_k ($k = 1,2,\ldots,M$) produces a CP of MN pulses with phases $\phi_j + \chi_k$. Similarly, we can design nested UNB CPs by nesting them into themselves. Also, one can create nested ultrapassband CPs, by nesting an UBB CP into an UNB CP or vice versa [20]. Such passband pulses may be used to stabilize the central peak of the UNB CPs, which in theory achieves a unit efficiency but in reality can have a lower peak value; nested ultrapassband CPs can stabilize this peak at the unit efficiency value.

We note also that the direct numerical simulation outperforms the nesting technique for a given number of constituent pulses. However, the nesting technique allows a very simple scaling procedure and trivial calculation of the phases, while the direct numerical procedure is computationally very demanding for long CPs.

The UBB CPs presented here are of potential interest in a variety of applications. For example, they can be used to accelerate sideband cooling of trapped ions [11]. Several dozen vibrational states are usually populated after Doppler cooling of the ions. The sideband cooling is conducted by the application of a laser field on the first red vibrational sideband of the electronic transition frequency. Because the red-sideband coupling depends on the number of phonons n, e.g., $\propto\sqrt{n}$ in the Lamb-Dicke regime, only a limited range of vibrationally dressed electronic states is efficiently excited in a single run. The UBB CPs allow us to excite many transitions simultaneously with nearly unit probability, e.g., the UB6 sequence of Table I can excite all sideband transitions with $n = 1$–100 with probability greater than 99%.

Another application is in optical pumping of atoms, where only a single polarized field is often used on the transition between the ground level and an excited level in order to prepare the atom in a well-defined magnetic sublevel of the ground level. The transitions between the magnetic sublevels of two levels with angular momenta J_1 and J_2 are proportional to the Clebsch-Gordan coefficients, which are different for each transition. For example, in the $J \leftrightarrow J$ transitions the largest and smallest Clebsch-Gordan coefficients differ by a factor of J and in the $J \leftrightarrow J-1$ transitions this ratio is $\sqrt{J(2J-1)}$. Hence all transitions between the magnetic sublevels in the $J_1 = 4 \leftrightarrow J_2 = 4$ and $J_1 = 4 \leftrightarrow J_2 = 3$ systems can be inverted simultaneously with over 99% probability by the UB4 and UB5 pulses from Table I, respectively.

It is important that the lower bound of the total pulse area $A_{\min}$ for the UBB CPs in Table I is in the range $2\pi - 5\pi$, even for an error value of 10^{-4}. The implication is that these UBB CPs require less pulse area and are therefore faster than adiabatic techniques, which typically require a pulse area of 10π and more. Moreover, these CPs deliver higher accuracy than adiabatic techniques.

ACKNOWLEDGMENTS

B.T.T. and N.V.V. acknowledge financial support from the EC Seventh Framework Programme under Grant Agreement No. 270843 (iQIT), the Alexander von Humboldt Foundation, and the Bulgarian National Science Fund Grant No. DMU-03/103. E.S.K. and B.T.T acknowledge financial support from a SUTD Start-Up Research grant, Project No. SRG EPD 2012 029, and an SUTD-MIT International Design Centre grant, Project No. IDG 31300102.

APPENDIX: ULTRABROAD-BAND AND ULTRANARROW-BAND COMPOSITE PULSE SEQUENCES

In this Appendix we present in Tables I–IV the specific values of the phases for the composite pulses derived and discussed in this paper.

TABLE I. Ultrabroad-band CPs composed of nonidentical pulses with different area, for an error value of $\epsilon = 0.01$, 0.001, and 0.0001. We denote the sequences by $(A_1)_{\phi_1}(A_2)_{\phi_2}\cdots(A_N)_{\phi_N}$, where A_k are the individual pulse areas and ϕ_k are the relative phases. Both A_k and ϕ_k are given in units π. Here $A_{\min}$ and $A_{\max}$ indicate the minimum and maximum total pulse areas of the high-fidelity window ($A_{\min},A_{\max}$), wherein $\mathcal{Q} < \epsilon$. The ratio $r = A_{\max}/A_{\min}$ is a measure of the dynamic range of the CP (i.e., its bandwidth in units of the minimum area $A_{\min}$). Note that for odd N the CPs are symmetric, while for even N they are asymmetric. Note also that our numerical code returned composite sequences in which the ratios between the individual pulse areas are rational numbers; we do not have an explanation for this fact.

CP	Composite sequence	$A_{\min}$	$A_{\max}$	r
	$\epsilon = 0.01$			
UB3	$(\alpha)_0,(\alpha)_{0.586\pi},(\alpha)_0$	1.65π	4.35π	2.63
UB4	$(\alpha)_0,(\alpha)_{0.454\pi},(\alpha)_{0.967\pi},(2\alpha)_{0.204\pi}$	1.96π	8.04π	4.10
UB5	$(\alpha)_0,(3\alpha)_{0.710\pi},(\alpha)_{1.351\pi},(3\alpha)_{0.710\pi},(\alpha)_0$	2.40π	15.60π	6.51
UB6	$(4\alpha)_0,(2\alpha)_{0.853\pi},(\alpha)_{0.289\pi},(\alpha)_{0.779\pi},(4\alpha)_{0.108\pi},(\alpha)_{1.333\pi}$	2.40π	23.60π	9.81
UB7	$(3\alpha)_0,(8\alpha)_{0.656\pi},(4\alpha)_{1.249\pi},(6\alpha)_{0.468\pi},(4\alpha)_{1.249\pi},(8\alpha)_{0.656\pi},(3\alpha)_0$	2.52π	33.48π	13.27
UB8	$(\alpha)_0,(8\alpha)_{0.658\pi},(4\alpha)_{0.906\pi},(16\alpha)_{1.994\pi},(8\alpha)_{0.833\pi},(4\alpha)_{0.292\pi},(12\alpha)_{0.823\pi},(9\alpha)_{1.955\pi}$	3.60π	58.40π	16.22
UB9	$(3\alpha)_0,(4\alpha)_{0.762\pi},(4\alpha)_{1.163\pi},(9\alpha)_{0.270\pi},(3\alpha)_{1.568\pi},(9\alpha)_{0.270\pi},(4\alpha)_{1.163\pi},(4\alpha)_{0.762\pi},(3\alpha)_0$	3.65π	82.34π	22.54

TABLE I. (*Continued*.)

CP	Composite sequence	$A_{\min}$	$A_{\max}$	r
	$\epsilon = 0.001$			
UB3	$(\alpha)_0,(\alpha)_{0.631\pi},(\alpha)_0$	2.06π	3.94π	1.91
UB4	$(\alpha)_0,(\alpha)_{0.556\pi},(\alpha)_{1.071\pi},(2\alpha)_{0.217\pi}$	2.81π	7.19π	2.56
UB5	$(\alpha)_0,(3\alpha)_{0.722\pi},(\alpha)_{1.387\pi},(3\alpha)_{0.722\pi},(\alpha)_0$	2.75π	15.25π	5.55
UB6	$(\alpha)_0,(6\alpha)_{0.681\pi},(2\alpha)_{0.409\pi},(6\alpha)_{1.347\pi},(6\alpha)_{0.627\pi},(\alpha)_{0.020\pi}$	3.25π	18.75π	5.77
UB7	$(\alpha)_0,(2\alpha)_{0.508\pi},(4\alpha)_{0.010\pi},(8\alpha)_{0.768\pi},(4\alpha)_{0.010\pi},(2\alpha)_{0.508\pi},(\alpha)_0$	2.77π	19.23π	6.94
UB8	$(4\alpha)_0,(2\alpha)_{0.881\pi},(\alpha)_{0.358\pi},(\alpha)_{1.861\pi},(4\alpha)_{0.774\pi},(2\alpha)_{1.842\pi},(2\alpha)_{0.144\pi},(\alpha)_{1.971\pi}$	3.62π	30.38π	8.38
UB9	$(3\alpha)_0,(\alpha)_{0.737\pi},(4\alpha)_{0.093\pi},(2\alpha)_{1.061\pi},(3\alpha)_{0.823\pi},(2\alpha)_{1.061\pi},(4\alpha)_{0.093\pi},(\alpha)_{0.737\pi},(3\alpha)_0$	4.12π	41.88π	10.17
	$\epsilon = 0.0001$			
UB3	$(\alpha)_0,(\alpha)_{0.651\pi},(\alpha)_0$	2.36π	3.64π	1.55
UB4	$(\alpha)_0,(\alpha)_{0.608\pi},(3\alpha)_{0.083\pi},(2\alpha)_{0.994\pi}$	4.58π	9.42π	2.06
UB5	$(\alpha)_0,(3\alpha)_{0.731\pi},(\alpha)_{1.392\pi},(3\alpha)_{0.731\pi},(\alpha)_0$	4.43π	13.57π	3.07
UB6	$(\alpha)_0,(2\alpha)_{0.754\pi},(\alpha)_{0.804\pi},(\alpha)_{1.470\pi},(3\alpha)_{0.782\pi},(\alpha)_{0.039\pi}$	3.29π	14.71π	4.47
UB7	$(\alpha)_0,(\alpha)_{0.741\pi},(2\alpha)_{0.437\pi},(3\alpha)_{1.749\pi},(2\alpha)_{0.437\pi},(\alpha)_{0.741\pi},(\alpha)_0$	3.40π	18.60π	5.48
UB8	$(4\alpha)_0,(2\alpha)_{0.914\pi},(\alpha)_{0.426\pi},(\alpha)_{1.927\pi},(4\alpha)_{0.816\pi},(2\alpha)_{1.854\pi},(2\alpha)_{0.116\pi},(\alpha)_{1.951\pi}$	4.58π	29.42π	6.42
UB9	$(3\alpha)_0,(\alpha)_{0.744\pi},(4\alpha)_{0.111\pi},(2\alpha)_{1.082\pi},(3\alpha)_{0.856\pi},(2\alpha)_{1.082\pi},(4\alpha)_{0.111\pi},(\alpha)_{0.744\pi},(3\alpha)_0$	4.83π	41.17π	8.53

TABLE II. Ultrabroad-band CPs composed of identical pulses with the same pulse area $\alpha_{\phi_1}\alpha_{\phi_2}\cdots\alpha_{\phi_N}$ for an error value of $\epsilon = 0.01$, 0.001, and 0.0001. For the sake of brevity, we list only the phases $(\phi_1,\phi_2,\ldots,\phi_N)$, which are given in units π. Here $\alpha_{\min}$ and $\alpha_{\max}$ indicate the minimum and maximum values of the high-fidelity window $(\alpha_{\min},\alpha_{\max})$, wherein $\mathcal{Q} < \epsilon$. The ratio $r = \alpha_{\max}/\alpha_{\min}$ is a measure of the dynamic range of the CP (i.e., its bandwidth in units of $\alpha_{\min}$). The three-pulse sequences are the same as in Table I and are given here for completeness. All CPs are symmetric.

CP	$(\phi_1,\phi_2,\ldots,\phi_N)$	$\alpha_{\min}$	$\alpha_{\max}$	r
	$\epsilon = 0.01$			
UB3*e*	$(0,0.586,0)\pi$	0.550π	1.450π	2.64
UB5*e*	$(0,0.653,0.416,0.653,0)\pi$	0.360π	1.640π	4.55
UB7*e*	$(0,0.673,0.550,0.849,0.550,0.673,0)\pi$	0.265π	1.735π	6.56
UB9*e*	$(0,0.167,0.848,0.525,0.450,0.525,0.848,0.167,0)\pi$	0.208π	1.792π	8.61
UB11*e*	$(0,0.428,0.476,1.026,0.674,0.381,0.674,1.026,0.476,0.428,0)\pi$	0.171π	1.829π	10.68
	$\epsilon = 0.001$			
UB3*e*	$(0,0.631,0)\pi$	0.688π	1.312π	1.91
UB5*e*	$(0,0.716,0.424,0.716,0)\pi$	0.476π	1.525π	3.20
UB7*e*	$(0,0.607,0.815,0.207,0.815,0.607,0)\pi$	0.357π	1.643π	4.60
UB9*e*	$(0,0.221,0.974,0.565,0.466,0.565,0.974,0.221,0)\pi$	0.284π	1.716π	6.05
UB11*e*	$(0,0.145,0.571,1.812,1.561,1.494,1.561,1.812,0.571,0.145,0)\pi$	0.235π	1.765π	7.52
	$\epsilon = 0.0001$			
UB3*e*	$(0,0.651,0)\pi$	0.786π	1.214π	1.55
UB5*e*	$(0,0.750,0.420,0.750,0)\pi$	0.576π	1.424π	2.47
UB7*e*	$(0,0.660,0.821,0.161,0.821,0.660,0)\pi$	0.442π	1.558π	3.53
UB9*e*	$(0,0.266,1.062,0.589,0.468,0.589,1.062,0.266,0)\pi$	0.356π	1.644π	4.63
UB11*e*	$(0,0.802,0.719,1.213,1.034,1.338,1.034,1.213,0.719,0.802,0)\pi$	0.296π	1.704π	5.77

TABLE III. Two-dimensional UBB CPs composed of nonidentical rectangular pulses with different pulse duration $(T_1)_{\phi_1}(T_2)_{\phi_2}\cdots(T_N)_{\phi_N}$, where T is measured in arbitrary time units τ and the phases are in units π. All CPs are symmetric.

CP	Composite sequence
UB3	$(0.415)_0,(1.586)_{0.616},(0.415)_0$
UB5	$(0.315)_0,(0.738)_{0.829},(1.771)_{1.317},(0.738)_{0.829},(0.315)_0$
UB5d	$(0.321)_0,(0.730)_{0.828},(1.728)_{1.320},(0.730)_{0.828},(0.321)_0$
UB5a	$(0.310)_0,(0.736)_{0.819},(1.779)_{1.292},(0.736)_{0.819},(0.310)_0$
UB7	$(0.259)_0,(0.654)_{0.902},(0.839)_{1.600},(1.781)_{1.972},(0.839)_{1.600},(0.654)_{0.902},(0.259)_0$
UB9	$(0.259)_0,(0.662)_{0.933},(0.856)_{1.706},(0.884)_{0.201},(1.133)_{0.374},(0.884)_{0.201},(0.856)_{1.706},(0.662)_{0.933},(0.259)_0$

TABLE IV. Ultranarrow-band composite sequences of identical pulses with the same pulse area $\alpha_{\phi_1}\alpha_{\phi_2}\dots\alpha_{\phi_N}$ for error values of $\epsilon = 0.01$, 0.001 and 0.0001. For the sake of brevity, we list only the phases of these CPs $(\phi_1,\phi_2,\dots,\phi_N)$. $\alpha_{\min}$ and $\alpha_{\max}$ indicate the borders of the no-transition windows $(0,\alpha_{\min})$ and $(\alpha_{\max},2\pi)$, wherein $\mathcal{P} < \epsilon$ (we have set $\alpha_{\max} = 2\pi - \alpha_{\min}$ in order to make the profiles symmetric). The ratio $r = \alpha_{\max}/\alpha_{\min}$ is a measure of the width of the CP, and lower values of r mean a better UNB CP.

CP	$(\phi_1,\phi_2,\dots,\phi_N)$	$\alpha_{\min}$	$\alpha_{\max}$	r
	$\epsilon = 0.01$			
UN3	$(0,0.587,1.174)\pi$	0.450π	1.550π	3.45
UN5	$(0,0.238,1.580,0.923,1.161)\pi$	0.637π	1.363π	2.14
UN7	$(0,0.124,1.820,0.502,1.183,0.879,1.003)\pi$	0.732π	1.268π	1.73
UN9	$(0,0.335,0.677,1.270,0.938,0.605,1.199,1.540,1.875)\pi$	0.788π	1.211π	1.54
UN11	$(0,0.281,0.313,1.784,0.100,0.597,1.094,1.411,0.883,0.917,1.200)\pi$	0.827π	1.173π	1.42
	$\epsilon = 0.001$			
UN3	$(0,0.631,1.262)\pi$	0.313π	1.687π	5.38
UN5	$(0,0.295,1.575,0.856,1.151)\pi$	0.520π	1.481π	2.85
UN7	$(0,0.612,0.409,1.796,1.182,0.980,1.591)\pi$	0.640π	1.360π	2.13
UN9	$(0,0.417,0.837,1.471,1.055,0.639,1.273,1.693,0.110)\pi$	0.713π	1.287π	1.81
UN11	$(0,0.776,0.859,1.313,1.472,1.744,0,0.153,0.576,0.643,1.399)\pi$	0.761π	1.239π	1.63
	$\epsilon = 0.0001$			
UN3	$(0,0.650,1.301)\pi$	0.215π	1.785π	8.28
UN5	$(0,0.332,1.580,0.828,1.160)\pi$	0.422π	1.578π	3.74
UN7	$(0,0.663,0.506,1.842,1.178,1.021,1.684)\pi$	0.555π	1.445π	2.60
UN9	$(0,0.478,0.959,1.610,1.132,0.654,1.306,1.786,0.265)\pi$	0.641π	1.359π	2.12
UN11	$(0,0.804,0.889,1.387,1.568,1.875,0.183,0.364,0.863,0.948,1.753)\pi$	0.702π	1.298π	1.85

[1] M. H. Levitt and R. Freeman, J. Magn. Reson. **33**, 473 (1979).
[2] R. Freeman, S. P. Kempsell, and M. H. Levitt, J. Magn. Reson. **38**, 453 (1980).
[3] M. H. Levitt, Prog. Nucl. Magn. Reson. Spectrosc. **18**, 61 (1986).
[4] R. Freeman, *Spin Choreography* (Spektrum, Oxford, 1997).
[5] S. S. Ivanov and N. V. Vitanov, Opt. Lett. **36**, 1275 (2011).
[6] G. T. Genov, B. T. Torosov, and N. V. Vitanov, Phys. Rev. A **84**, 063413 (2011); G. T. Genov and N. V. Vitanov, Phys. Rev. Lett. **110**, 133002 (2013).
[7] B. T. Torosov and N. V. Vitanov, Phys. Rev. A **83**, 053420 (2011).
[8] B. T. Torosov, S. Guérin, and N. V. Vitanov, Phys. Rev. Lett. **106**, 233001 (2011).
[9] D. Schraft, T. Halfmann, G. T. Genov, and N. V. Vitanov, Phys. Rev. A **88**, 063406 (2013).
[10] G. T. Genov, D. Schraft, T. Halfmann, and N. V. Vitanov, Phys. Rev. Lett. **113**, 043001 (2014).
[11] F. Schmidt-Kaler, H. Haffner, M. Riebe, S. Gulde, G. P. T. Lancaster, T. Deuschle, C. Becher, C. F. Roos, J. Eschner, and R. Blatt, Nature (London) **422**, 408 (2003); M. Riebe, T. Monz, A. S. Villar, P. Schindler, M. Chwalla, M. Hennrich, and R. Blatt, Nat. Phys. **4**, 839 (2008); T. Monz, K. Kim, W. Hansel, M. Riebe, A. S. Villar, P. Schindler, M. Chwalla, M. Hennrich, and R. Blatt, Phys. Rev. Lett. **102**, 040501 (2009).
[12] M. Pons, V. Ahufinger, C. Wunderlich, A. Sanpera, S. Braungardt, A. Sen(De), U. Sen, and M. Lewenstein, Phys. Rev. Lett. **98**, 023003 (2007); N. Timoney, V. Elman, S. Glaser, C. Weiss, M. Johanning, W. Neuhauser, and C. Wunderlich, Phys. Rev. A **77**, 052334 (2008); C. Piltz, B. Scharfenberger, A. Khromova, A. F. Varon, and C. Wunderlich, Phys. Rev. Lett. **110**, 200501 (2013).
[13] S. S. Ivanov and N. V. Vitanov, Phys. Rev. A **84**, 022319 (2011).
[14] R. Tycko and A. Pines, Chem. Phys. Lett. **111**, 462 (1984).
[15] R. Tycko, Phys. Rev. Lett. **51**, 775 (1983).
[16] S. Wimperis, J. Magn. Reson. **109**, 221 (1994).
[17] A. J. Shaka and R. Freeman, J. Magn. Reson. **59**, 169 (1984).
[18] R. Tycko, A. Pines, and J. Guckenheimer, J. Chem. Phys. **83**, 2775 (1985).
[19] N. V. Vitanov, Phys. Rev. A **84**, 065404 (2011).
[20] E. Kyoseva and N. V. Vitanov, Phys. Rev. A **88**, 063410 (2013).
[21] H. M. Cho, R. Tycko, A. Pines, and J. Guckenheimer, Phys. Rev. Lett. **56**, 1905 (1986).
[22] B. T. Torosov and N. V. Vitanov, Phys. Rev. A **87**, 043418 (2013).
[23] B. W. Shore, *The Theory of Coherent Atomic Excitation* (Wiley, New York, 1990).